Structural Analysis of the Photosystem I Supercomplex of Cyanobacteria Induced by Iron Deficiency†

Jon Nield, Edward P. Morris, Thomas S. Bibby, and James Barber*

Wolfson Laboratories, Department of Biological Sciences, Imperial College of Science, Technology and Medicine, London SW7 2AZ, U.K.

Received October 1, 2002; Revised Manuscript Received January 7, 2003

ABSTRACT: Here we describe the three-dimensional structure of the newly discovered CP43′−photosystem I (PSI) supercomplex of cyanobacteria calculated by single-particle analysis of images obtained by electron cryomicroscopy (cryo-EM). This large membrane protein complex has a molecular mass of approximately 2 MDa and is found in cyanobacteria when grown in iron deficient media. It is composed of a reaction center trimer surrounded by 18 subunits of the chlorophyll *a* binding CP43′protein, encoded by the *isiA* gene, which increases the light harvesting capacity of PSI by ∼70%. By modeling higher-resolution structural data obtained from X-ray crystallography into the three-dimensional (3D) cryo-EM map, we have been able to gain a better understanding of the structure and functional properties of this supermolecular complex. We have identified three separate clusters of chlorophyll molecules at the periphery of the PSI core which may aid energy transfer from the CP43′ antenna ring to the reaction center. Moreover, it is shown that despite the replacement of ferredoxin with flavodoxin as an electron acceptor under iron stress conditions, the 3D map has density to accommodate the extrinsic proteins, PsaC, PsaD, and PsaE. The presence of these three proteins was also confirmed by immunoblotting.

Given that iron is often in limited supply in oxygenic aquatic ecosystems (*1*, *2*) due mainly to the insolubility of Fe^{3+} salts at neutral pH, it is not surprising that microorganisms such as cyanobacteria have developed mechanisms for compensating for this (*3*). Iron is an essential component of a host of enzymes and, in particular, plays a central role in the redox activity of the respiratory and photosynthetic electron transport chains. In the case of cyanobacteria, iron deficiency activates the expression of two iron stress-induced genes, isiA and isiB (*4*, *5*). Often the two genes are located on the same operon and can be transcribed both monocistronically and dicistronically (*6*).

The *isi*B gene encodes flavodoxin which replaces the iron-containing ferredoxin as an electron acceptor for photosystem I (PSI)[1] (*7*). The *isi*A gene encodes the IsiA protein, often called CP43′ because it has an amino acid sequence homologous to that of the chlorophyll *a*-binding protein CP43 of photosystem II (PSII) (*8*, *9*). This similarity suggests that CP43′ has six transmembrane helices and binds approximately the same number of chlorophyll *a* (Chl*a*) molecules as CP43 does (*10*). However, the two proteins differ in molecular mass since CP43′ has ∼130 fewer amino acids than CP43 due to the absence of a large hydrophilic loop joining the lumenal ends of transmembrane helices 5 and 6. For *Synechocystis* PCC 6803, CP43′ has a calculated molecular mass of 37 221 Da as compared with a mass of 51 760 Da for CP43.

Although there had been several suggestions for the functional role of CP43′, it was only recently discovered that 18 copies of this protein form a well-structured light-harvesting antenna ring around the trimeric reaction center of *Synechocystis* PCC 6803 (*11*) and *Synechococcus* PCC 7942 (*12*). The resulting CP43′−PSI supercomplex has a molecular mass in the region of 2 MDa and has 234 Chls bound within the antenna ring, assuming each CP43′ subunit binds 13 Chl*a* molecules like CP43 does according to recent X-ray analyses (*13*, *14*).[2] Both fluorescence (*15*) and absorption (*12*) studies indicated that these Chls are functionally coupled to Chl*a* of the PSI reaction center trimeric core and therefore increase the light harvesting capacity of PSI by ∼70%. This increase in the antenna size of PSI is probably a response to the lowering of the phycobiliprotein level and a decrease in the PSI:PSII ratio when cyanobacteria are iron-stressed (*17*, *18*).

The structure of the CP43′−PSI supercomplex was first visualized by electron microscopy after staining with uranyl acetate using single-particle analyses (*11*, *12*, *15*). The presence of heavy metal stain may, however, distort certain structural features (*19*). Therefore, to obtain a more reliable structure of the CP43′−PSI supercomplex and thereby gain further insight into how the CP43′ antenna ring and its Chls interact with the trimeric PSI reaction center core, we have calculated a three-dimensional (3D) structure using electron cryomicroscopy (cryo-EM). To do so, the sample was rapidly frozen in its hydrated state in vitreous ice without the presence of heavy metal stain. The supercomplexes were visualized as randomly oriented particles in a high-voltage

† This work was supported by the Biotechnology and Biological Sciences Research Council (BBSRC). J.N. holds a Royal Society University Research Fellowship.

* To whom correspondence should be addressed. Telephone: +44 20 75945266. Fax: +44 20 75945267. E-mail: j.barber@ic.ac.uk.

[1] Abbreviations: Chl, chlorophyll; CTF, contrast transfer function; EM, electron microscopy; FEG, field emission gun; PAGE, polyacrylamide gel electrophoresis; PSI, photosystem I; PSII, photosystem II.

[2] Just prior to the publication of this paper, a new structure of PSII was reported (*35*) which confirmed that CP43 binds 13 Chl*a* molecules.

10.1021/bi026933k CCC: $25.00
Published on Web 03/04/2003

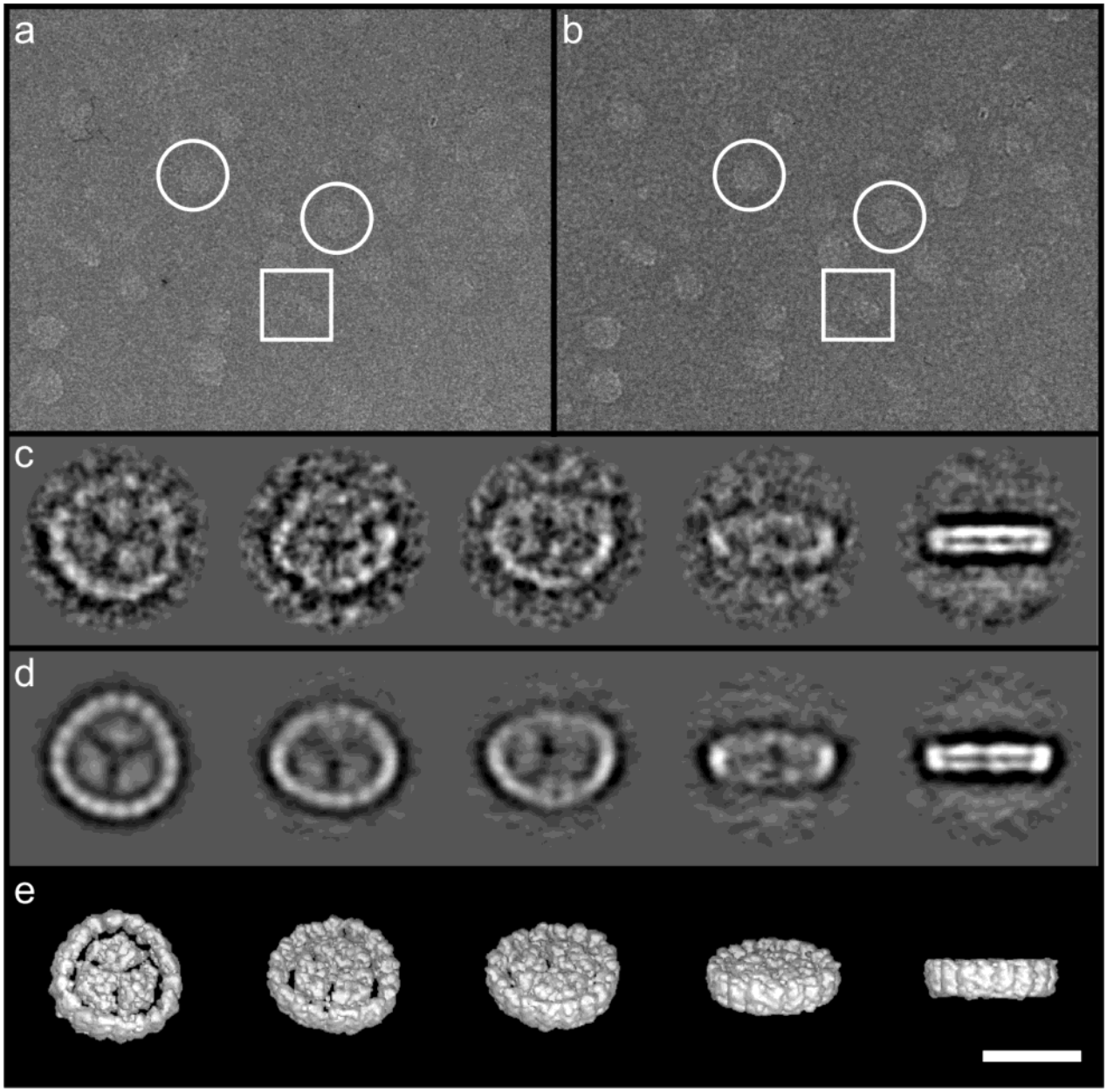

FIGURE 1: Electron micrographs of typical preparations of the CP43′−PSI supercomplex isolated from *Synechocystis* PCC 6803 showing particles randomly oriented in vitreous ice: (a) near to focus at ~2.5 μm and (b) underfocused at ~5 μm. (c) Selection of typical class averages used for the 3D reconstruction. (d) Reprojections from the 3D map in orientations identical to those corresponding class averages in panel c. (e) Surface representation of the final 3D map viewed in the same orientation as the class averages. The scale bar is 300 Å.

electron microscope equipped with a field emission gun (FEG). The images of the supercomplexes were then processed and merged to generate a 3D model of the CP43′−PSI supercomplex at a resolution of ~20 Å. Since this new structure of the CP43′−PSI supercomplex directly represents protein density rather than visualizing the imprint left by negative stain, it provides a more accurate framework for the incorporation of recent higher-resolution structural information derived from X-ray crystallography.

MATERIALS AND METHODS

Preparation of the Supercomplex. The CP43′−PSI supercomplex was isolated from a mutant of the cyanobacterium *Synechocystis* PCC 6803 having a histidine tag engineered into the carboxy terminus of the PSII chlorophyll *a*-binding protein, CP47 (*20*), using the procedure reported previously (*11*, *15*). The polypeptides of the extrinsic proteins of PSI were resolved by SDS−PAGE and immunoblotted with antibodies raised to PsaC, PsaD, and PsaE (a kind gift from J. Golbeck, The Pennsylvania State University, University Park, PA) using a method similar to that described previously (*21*).

Electron Cryomicroscopy. Samples of the CP43′−PSI supercomplex were applied to glow-discharged carbon-coated grids and rapidly frozen in liquid ethane. The grids were transferred to a Philips CM200 FEG electron microscope equipped with a Gatan liquid N_2 cryostage operated at −184 °C. Low-dose images were recorded at an accelerating voltage of 200 kV using a calibrated magnification of 38400× and defocus levels of ~2.5 and ~5 μm.

Image Processing. Electron micrographs were digitized using a Leafscan 45 densitometer at a step size of 10 μm.

Subsequent image processing was conducted using Imagic 5 programs (*22*, *23*) and locally developed software. The pixel size of scanned images was coarsened by a factor of 2 by averaging patches of 2 × 2 pixels so that the effective sampling at the specimen level was 5.263 Å. A data set of 4400 molecular images was selected interactively and corrected for the effects of the contrast transfer function (CTF) by phase reversal in zones of reversed contrast using defocus values measured from the observed Thon rings in the power spectra of the negatives. Molecular images were aligned, classified, and averaged using standard Imagic procedures (*19*, *23*). The resulting class averages were assigned Euler angles by angular reconstitution (*24*) and back projected to calculate the 3D density distribution. 3D maps calculated in this way were used to refine the initial alignment, classification, and Euler angle assignment. This refinement procedure was repeated several times.

Molecular Modeling. Molecular models of the CP43′−PSI supercomplex were built using the program O (*25*). Coordinate sets derived from the 2.5 Å crystallographic structure of cyanobacterial PSI (*26*), deposited in the Protein Data Bank as entry 1JB0, and the 3.8 Å crystallographic structure of PSII (*13*), deposited as PDB entry 1FE1, were fitted by visual inspection into the electron microscope-derived 3D density maps.

RESULTS

Calculation of the 3D Structure. CP43′−PSI supercomplexes, isolated from the thylakoid membranes of *Synechocystis* PCC 6803 by sucrose density centrifugation (*11*, *15*), were rapidly frozen onto carbon film. The supercomplex images were recorded at two focal levels, nearer to focus (∼2.5 μm defocus) and further from focus (∼5 μm defocus) (Figure 1a,b). From processing a data set of 4400 CTF-corrected particles, the final 3D reconstruction that was obtained involved merging 150 class averages that displayed a greatly improved signal-to-noise ratio over the raw data set of particle images. Construction of this 3D map involved iterative refinement and exploited the observed 3-fold symmetry. Five characteristic class average views of the CP43′−PSI supercomplex are shown in Figure 1c. The relative orientations were determined for each class average and were used to construct the cryo-EM 3D map (Figure 1e) and the corresponding calculated reprojections (Figure 1d). Fourier-shell correlation gave a resolution of 20 Å for the 3D model. Figure 2a shows a surface representation of an oblique view of the 3D model. The overall maximum dimensions are 320 Å (width) and 90 Å (thick). These dimensions compare with the values of 330 and 80 Å, respectively, previously deduced from a 24 Å 3D model of the CP43′−PSI supercomplex obtained from single-particle analysis of negatively stained samples (*15*). The difference, in part, reflects the detection of the detergent shell by the negative stain and dehydration effects that are minimized by the cryo-EM approach. Moreover, the cryo-EM structure gives details of protein distribution without interference of density features introduced by negative staining. The improved quality of the density distribution within the three central PSI monomers, compared with the earlier 3D map (*15*), allowed the unambiguous assignment of the stromal and lumenal surfaces. The two-dimensional (2D) projection map viewed from the stromal surface shown in Figure 2b illustrates the more reliable representation of the relative structural relationships between the 18-member CP43′ antenna ring and the central trimeric PSI reaction center core, compared to that previously available. The internal features display a clear polarity within each PSI monomer, and the central triangular linking region of the trimer is well-defined. The CP43′ subunits appear as triangular densities, with six forming an arc around the edge of each PSI monomer. Figure 2b is the first direct visualization of a reliable spatial relationship between the CP43′ ring and the central trimeric reaction center core of the iron stress-induced supercomplex.

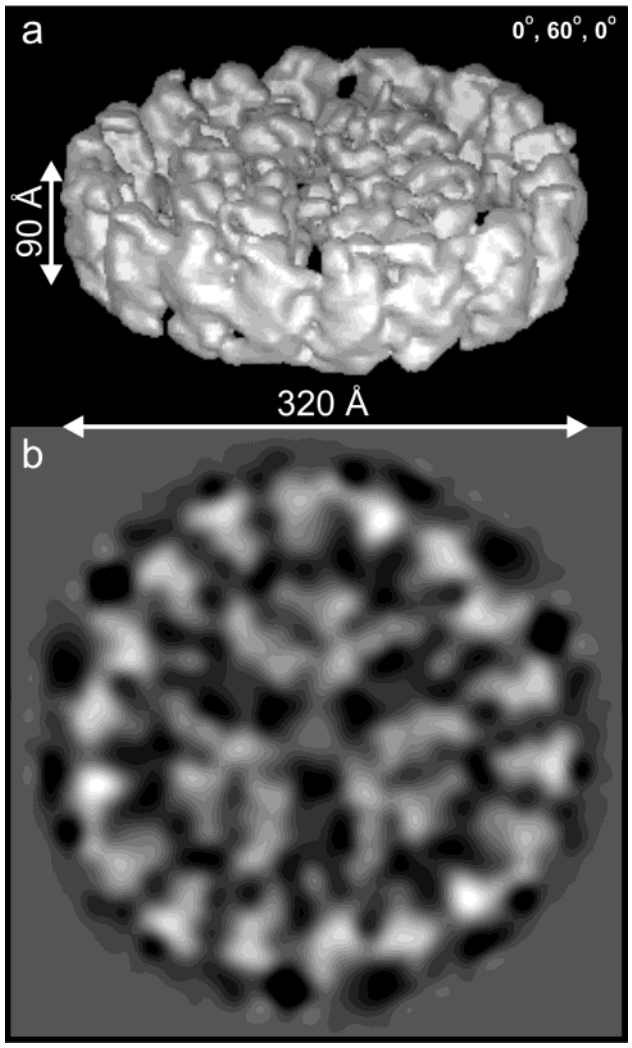

FIGURE 2: Cryo-EM map of the CP43′−PSI supercomplex at approximately 20 Å resolution. (a) Surface representation of the 3D structure shown at an oblique angle. (b) Top view 2D projection map.

Modeling of X-ray Data into the 3D Map. As emphasized above, the cryo-EM structure provides a significantly improved framework in which higher-resolution X-ray data can be modeled. Figure 3 shows that the recently published coordinates of the 2.5 Å X-ray structure of the PSI trimer of the cyanobacterium *Synechococcus elongatus* (*26*) fit reasonably well into the central region of the supercomplex with good correspondence between the distribution of density in the 20 Å cryo-EM map and the X-ray data. In the case of

FIGURE 3: Modeling of the C_α backbone and chlorophylls (yellow) of the PSI trimer (green) and CP43 helices (red) using data derived from X-ray diffraction studies (*13*, *26*) into the 3D cryo-EM map viewed from the stromal side.

CP43′, there is no high-resolution structure, but recently, a 3.8 Å model of the six transmembrane helices of CP43 has become available from X-ray diffraction analyses of 3D crystals of the PSII core dimer of the cyanobacterium *S. elongatus* (*13*, *14*). Given that the CP43′ and CP43 proteins are expected to be structurally homologous at the level of transmembrane helices (*10*, *15*), we have used the X-ray data of CP43 to model CP43′ into 18 densities attributed to this protein. The modeling shown in Figure 3 is consistent with the distribution of density for a CP43 subunit, but at this resolution, the accurate incorporation of individual transmembrane helices for each CP43′ was not possible. However, in Figure 3 we have chosen to model transmembrane helices 5 and 6 of CP43′ immediately adjacent to the PSI reaction center core since the same pair of helices of CP43 are located close to the PSII D1 and D2 reaction center proteins (*13*, *27*).

Organization of Chlorophyll Molecules. Incorporation of the X-ray structures into the 3D cryo-EM map allowed the development of a model for the organization of the Chl*a* molecules bound within the CP43′−PSI supercomplex as shown in Figure 4. According to X-ray analyses, each monomeric PSI reaction center core of *S. elongatus* binds 96 Chl*a* molecules, including those involved in primary charge separation. The precise positioning and numbers of Chl*a* molecules bound to CP43 are less certain, although the 3.8 Å X-ray structure of PSII presented here has assigned densities to 12 Chl*a* molecules (*13*). This value has been subsequently increased to 13 (*14*). The assigned positions of the Chl*a* molecules have been assumed to be the same in

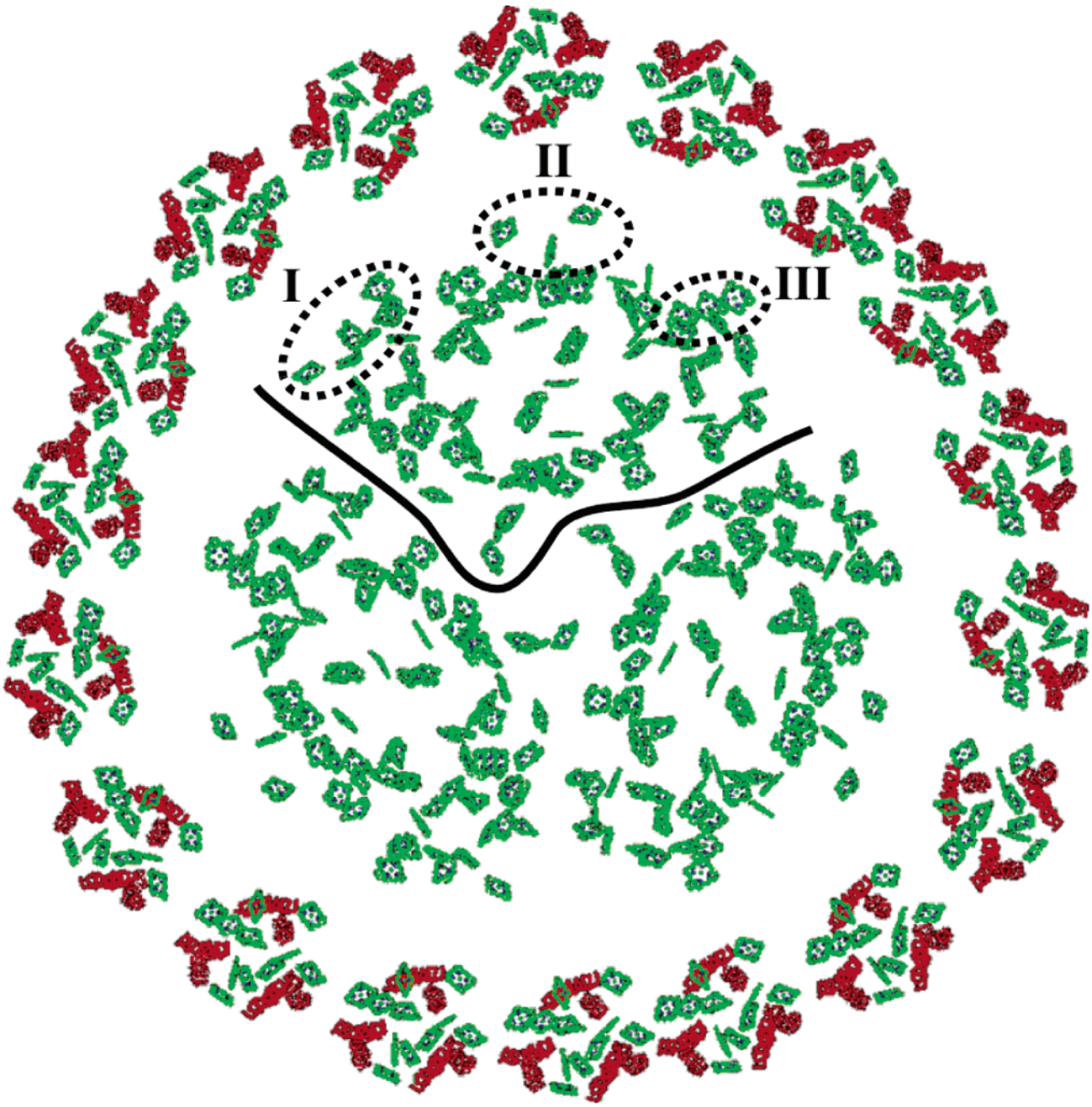

FIGURE 4: Modeling of the chlorophyll organization of the CP43′−PSI supercomplex using coordinates from the 2.5 Å X-ray PSI trimer structure (*26*) and 3.8 Å PSII CP43 structure (*13*). The chlorophylls of the PSI trimer and CP43′ are in green, and the transmembrane helices of CP43′ are in red. The supercomplex is viewed from the stromal side. The three ringed regions (I−III) highlight regions where the peripheral chlorophylls of a PSI reaction center monomer are closest to the chlorophylls within the CP43′ ring. This modeling has assumed that helices 5 and 6 of CP43′ are adjacent to the surface of the PSI reaction center.

CP43′ and are incorporated into Figure 4. We also assume that the organization of Chls in the PSI reaction centers of *S. elongatus* and *Synechocystis* is the same, which may not be so (*28*). With these assumptions in mind, the modeling suggests three regions (circled I, II, and III in Figure 4) where Chl*a* molecules located toward the outer surface of the PSI reaction center core are within 20−25 Å of Chl*a* molecules bound within CP43′ subunits and which may be important in transferring excitation energy from the antenna ring to the reaction center.

The peripheral Chl*a* molecules within the circled regions are shown in more detail in Figure 5. The numbering of these Chl*a* molecules is in accordance with the literature (*29*), and also given in the text in brackets are their PDB "resName" descriptors. The first circled region (region I) contains a cluster of seven Chls, of which three are distributed toward the stromal surface, A8, A10, and A18 (CL1108, CL1110, and CL1118, respectively), and three toward the lumenal surface, A12−A14 (CL1112−CL1114, respectively). All are located within the transmembrane helices of the PsaA protein spanning the region from A-Gly170 to A-Gly320, and all are ligated to histidines. Interestingly, the seventh Chl*a* of this cluster, K2 (CL1402), is coordinated with the small subunit PsaK at residue K-His67. The central cluster (region II) contains three chlorophylls, J1−J3 (CL1301−CL1303, respectively) which are associated with the small subunit

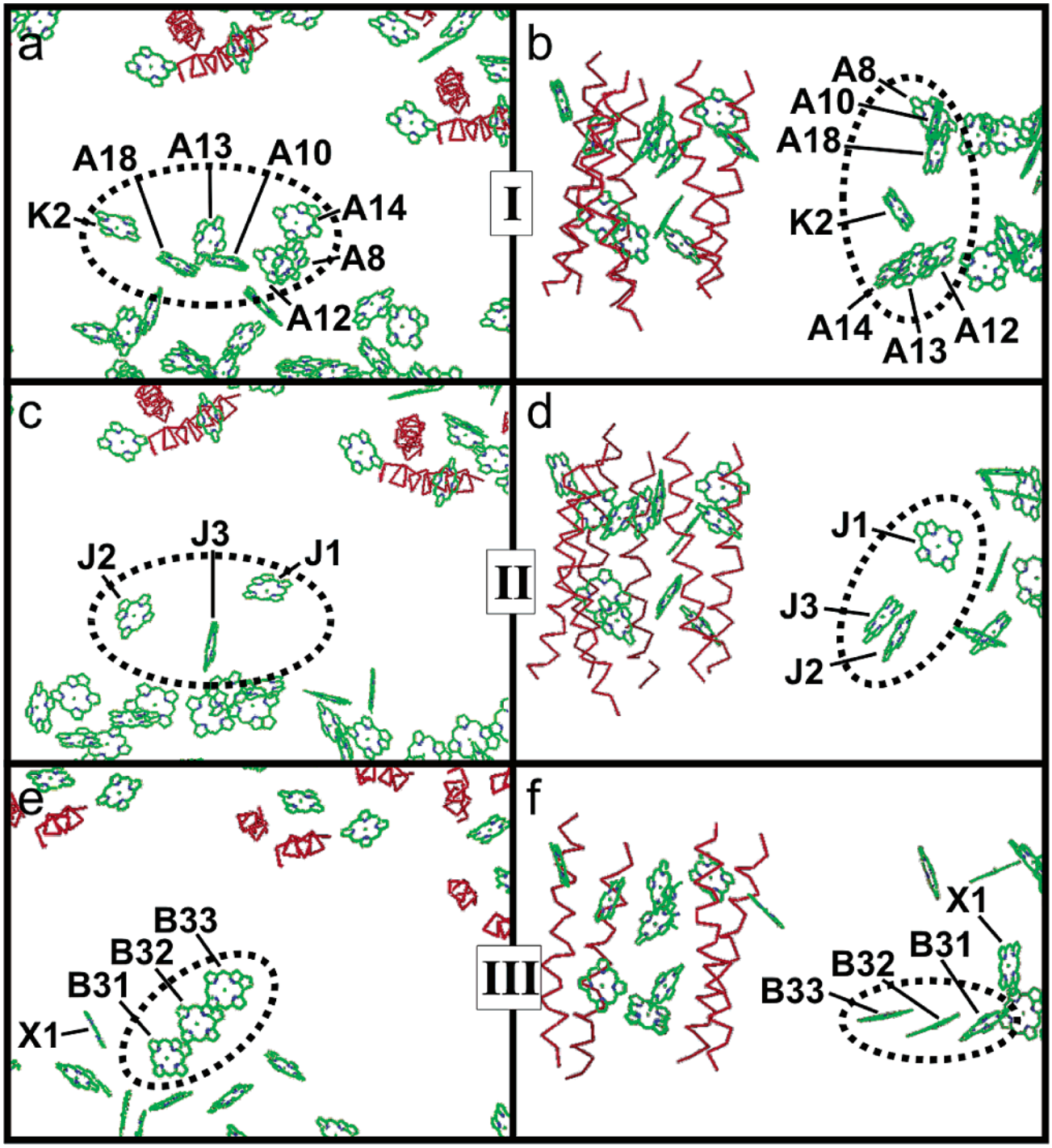

FIGURE 5: Close-up top views from the stromal surface (a, c, and e) and side views (b, d, and f) of the highlighted regions (I, II, and III) identified in Figure 4. The chlorophylls are numbered according to the method of Byrdin et al. (*29*).

PsaJ. Chl J2 is ligated to J-Glu28 and J3 to J-His39. The other chlorophyll, J1, is ligated to a water molecule also coordinated with the PsaJ protein. The cluster of Chls identified in region III is composed of three Chl*a* molecules, B31−B33 (CL1231−CL1233, respectively), each separated by ~8 Å, lying almost in the plane of the membrane toward the lumenal side. All are directly or indirectly ligated to a large lumenal loop of the PsaB protein stretching from residue B-Phe465 to B-Gly510. Chlorophyll B31 is ligated to B-His470, and the other chlorophylls, B32 and B33, are coordinated to water molecules. However, there is some uncertainty about whether these clusters of Chls exist in *Synechocystis* (*28*).

If it is assumed that the PSI structure of *S. elongatus* applies for *Synechocystis*, it seems likely that the three clusters of Chls identified in regions I−III could facilitate energy transfer from the CP43′ antenna ring to the PSI reaction center. Although some of these Chls are associated with the PsaA and PsaB reaction center proteins, some are linked with the small subunit located on the peripheral edge of the trimer. This is clearly the case for all three Chls associated with PsaJ and similarly for one of the Chls indirectly coordinated with PsaK.

Extrinsic Proteins Involved in Ferredoxin or Flavodoxin Binding. When cyanobacteria are grown in a medium containing a plentiful supply of iron, ferredoxin acts as an

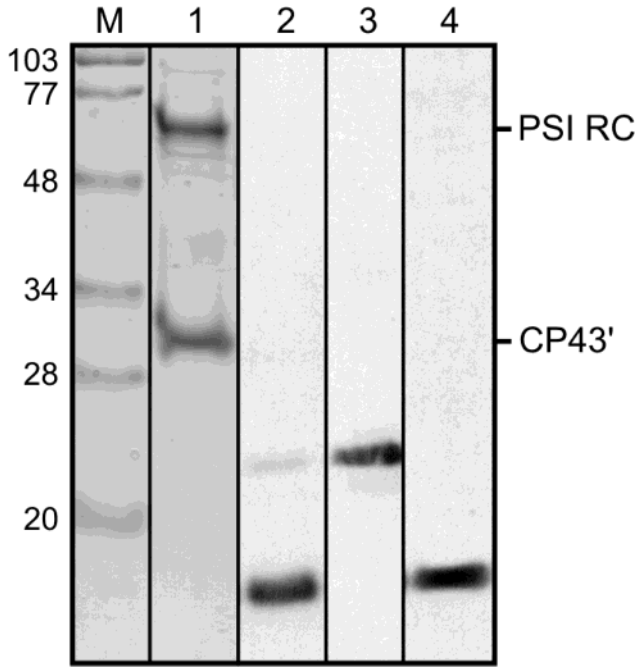

FIGURE 6: Identification of the presence of the extrinsic PsaC, PsaD, and PsaE proteins in the CP43′−PSI supercomplex by immunoblotting: lane M, molecular mass markers; lane 1, SDS−PAGE profile of the CP43′−PSI complex; and lanes 2−4, immunoblots for PsaC, PsaD, and PsaE, respectively. The positions of the PSI reaction center proteins, PsaA and PsaB (PSI-RC), and CP43′ are marked.

electron acceptor for PSI (*30*, *31*). Under these conditions, PSI has three subunits attached to its stromal surface, which are PsaC (containing two iron−sulfur centers, F_A and F_B), PsaD, and PsaE (*26*). It is believed that the latter two facilitate the binding of soluble ferredoxin. However, under iron deprivation, ferredoxin is functionally replaced with flavodoxin (*7*). Therefore, it is conceivable that under iron stress conditions there may be some alteration to the complement of extrinsic proteins normally present at the stromal surface of PSI. However, studies conducted on PSI trimers isolated from *Synechococcus* PCC 7002 grown under iron-limiting conditions indicated that all extrinsic proteins were present and were required for the efficient binding of flavodoxin (*32*). Surprisingly, this study did not report the presence of the CP43′−PSI supercomplex. A later study, using *Synechococcus* PCC 7942, identified the iron stress-induced CP43′−PSI supercomplex and also the presence of extrinsic proteins (*12*). As shown in Figure 6, an immunological analysis conducted on the isolated CP43′−PSI supercomplex of *Synechocystis* confirmed that all three extrinsic proteins were present. In agreement with this, when thin sections of the 3D structure are viewed from the top toward the stromal surface (Figure 7a) and looking from the side (Figure 7b), the density present is able to accommodate most of the three extrinsic proteins, as emphasized by incorporating the published X-ray structure of PSI (*26*) into the cryo-EM map. This therefore establishes that the biochemically detected extrinsic proteins are indeed components of the CP43′−PSI supercomplex.

The fitting of CP43′ is based on the C_α backbone of the six transmembrane helices of the CP43-derived PSII X-ray model of Zouni et al. (*13*). In the case of CP43′, this represents approximately one-third of the protein mass (*15*). The remaining two-thirds is approximately equally distributed between the stromal and lumenal extrinsic domains. Therefore, the additional densities making up the stromal and lumenal surfaces of the CP43′ ring as shown in Figure 7b are due to the extrinsic loops joining the transmembrane helices of CP43′.

DISCUSSION

When the cyanobacterium *Synechocystis* PCC 6803 is deprived of iron in its growth medium, a giant supercomplex composed of the PSI reaction center trimer surrounded by 18 subunits of CP43′ is formed (*11*). A similar supercomplex has been identified in *Synechococcus* PCC 7942 (*12*). The formation of this supercomplex seems to compensate for the lowering of the overall level of PSI relative to PSII and for a reduction in phycobiliprotein levels that occur when the availability of iron is limited (*17*, *18*). Previous structural studies have involved staining with uranyl acetate to aid visualization of the supercomplex in the electron microscope (*11*, *12*, *15*). Here we present a structural model determined in vitreous ice at liquid nitrogen temperatures in the absence of negative stain. To visualize the supercomplex under these conditions, we have employed a high-voltage electron microscope equipped with a field emission gun. We estimate the resolution of the structure to be ~20 Å. The surrounding CP43′ subunit ring is not exactly circular, being distorted by the inner trimer. How the antenna ring is stabilized by protein−protein interactions is unclear at the present resolution. However, the interactions between the adjacent CP43′ subunits within the antenna ring seem to be tighter than those between the ring and the central PSI trimer.

The cryo-EM map has allowed us to model, with some confidence, the latest high-resolution coordinates of the X-ray structure of the PSI trimer of *S. elongatus* (*26*). In so doing, we have assumed that the Chl organization in this organism is the same in *Synechocystis*. Bearing this in mind, we have identified Chl molecules that are associated with low-molecular weight subunits, particularly PsaJ and possibly PsaK. However, in the case of PsaX, genome analyses suggest that *Synechocystis* PCC 6803 does not contain this protein which in *S. elongatus* binds one chlorophyll molecule. If present in *Synechocystis*, then its chlorophyll X1 (CL1701) would be in region III, adjacent to the third inner chlorophyll B31 (CL1231) of the cluster of three in this region and more than 30 Å from the CP43′ ring.

The X-ray structure also revealed that the low-molecular weight proteins, PsaL and PsaM, located at the center of the PSI trimer also bind chlorophyll (*26*). It seems likely that these centrally located low-molecular weight chlorophyll-binding subunits facilitate energy transfer between the monomeric PSI complexes of the trimer. In the case of PsaL, its presence is also required for the stabilization of the trimer (*33*). Thus, it seems that the role of the Chl*a* molecules bound to the low-molecular weight proteins of PSI is mainly to aid energy transfer between the adjacent major subunits that make up the giant supercomplex.

In the absence of a high-resolution structure of CP43′, it is not possible to conduct a detailed simulation of energy transfer within the CP43′ ring or from the ring to the reaction center trimer. However, recent femtosecond and picosecond

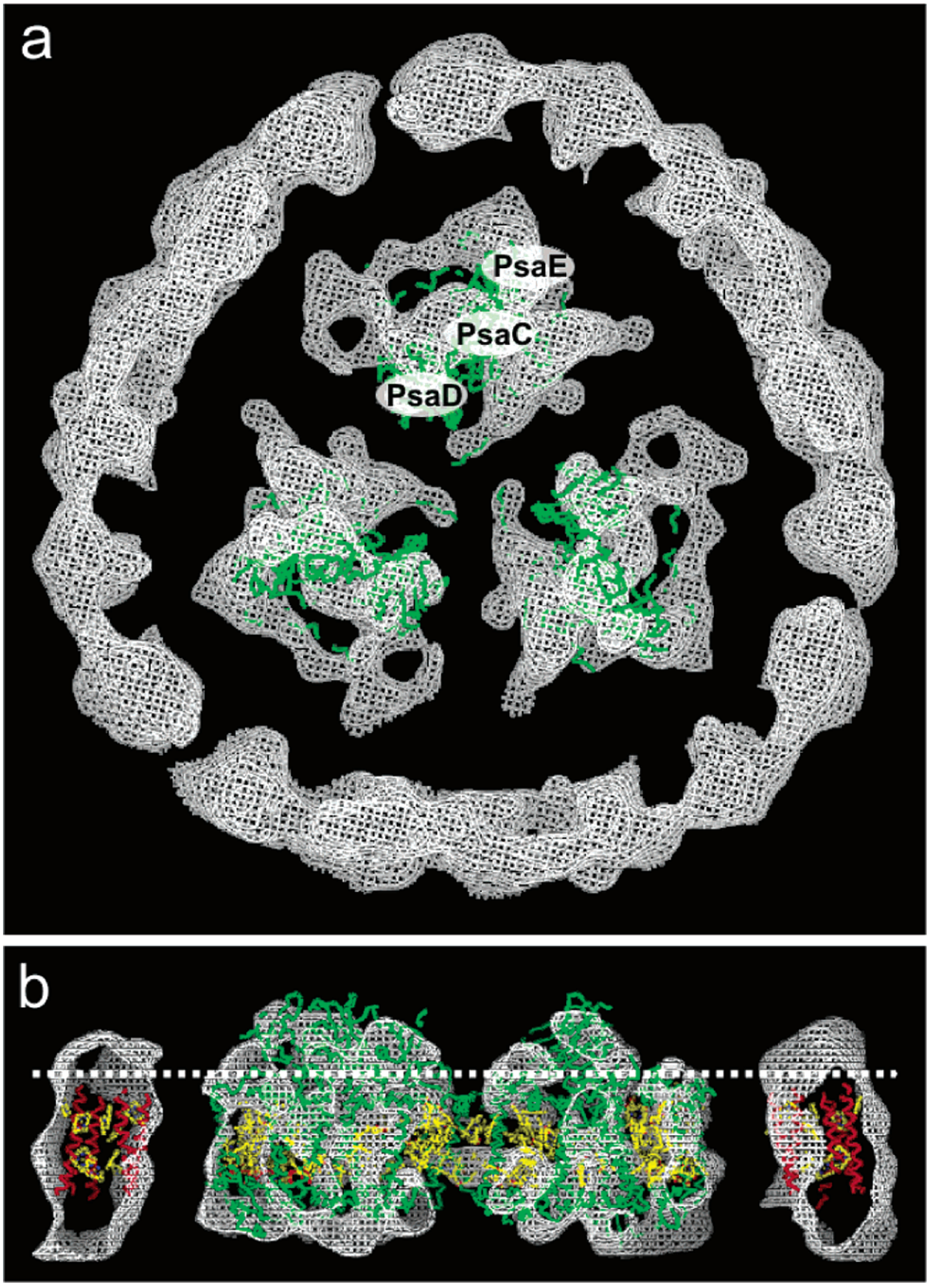

FIGURE 7: Presence of the PsaC, PsaD, and PsaE proteins in the 3D cryo-EM map of the CP43′−PSI supercomplex. (a) A 25 Å slice of the stromal surface (all density above the dashed white line in panel b) emphasizes the density attributed to the PsaC, PsaD, and PsaE extrinsic proteins. (b) A 20 Å cross section in side view further emphasizes this density. C_α backbones are colored green for the PSI trimer and red for the CP43 helices. Chlorophylls are yellow.

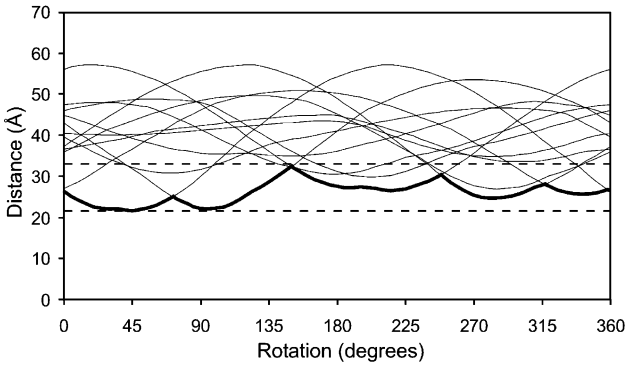

FIGURE 8: Distance of closest approach between the J3 chlorophyll of PSI and the putative chlorophylls in the neighboring CP43′ subunit. Edge to edge distances between the J3 chlorophyll and each of the 12 putative chlorophylls in CP43′ (continuous black lines) are shown as a function of rotation of CP43′ about an axis through the center of mass of the subunit normal to the plane of the membrane. The distance of closest approach (boldest continuous black line) lies between limits (dashed lines) corresponding to 22 and 33 Å.

optical absorption and fluorescence transient spectroscopy (*34*) and other studies (*12*, *15*, *16*) have shown that energy is transferred from the antenna ring to the reaction center very efficiently. We estimate that the shortest Chl−Chl distance between neighboring CP43′ subunits of the antenna ring is ∼10 Å, which suggests that energy transfer within the ring could be extremely rapid compared to the rate of transfer to the reaction center core, estimated to be within a few picoseconds by Melkozernov and colleagues (*34*). Although we have modeled CP43′ placing transmembrane helices 5 and 6 close to the reaction center core, the Chl−Chl distances either between the adjacent CP43′ subunits or between the antenna ring and the reaction center core do not vary significantly by rotating the six transmembrane helices within the assigned density. This is emphasized in Figure 8, where we have rotated the CP43 X-ray model within the density assigned to CP43′ and show that the closest edge to edge distance between the J3 Chl and the Chls of CP43′ vary between 22 and 33 Å. Similar results were obtained when other peripheral Chls were chosen and subjected to the same analysis.

The structural model presented here not only provides a framework to allow interpretation of energy transfer measurements but also gives a basis for mutagenesis studies, directed either at the small subunits or at the ligands binding the peripheral chlorophylls of PsaA and PsaB.

Finally, we have observed that despite the dramatic effect of iron deficiency on the PSI level, and the change in its functional electron acceptor, it continues to assemble a reaction center complex containing the extrinsic PsaC, PsaD, and PsaE proteins which presumably aid the binding and reduction of flavodoxin.

ACKNOWLEDGMENT

Discussions with our various colleagues, particularly Marin van Heel, have been much appreciated.

REFERENCES

1. Martin, J. H., Coale, K. H., Johnson, K. S., Fitzwater, S. E., Fordan, R. M., Tanner, S. J., Hunter, C. N., Elrod, V. A., Nowicki, J. L., Coely, T. L., et al. (1994) *Nature 371*, 123−129.
2. Behrenfeld, M. J., and Kolber, Z. S. (1999) *Science 283*, 840−843.
3. Straus, N. A. (1994) in *The Molecular Biology of Cyanobacteria* (Bryant, D. A., Ed.) pp 731−750, Kluwer Academic Press, Dordrecht, The Netherlands.
4. Pakrasi, H. B., Goldenberg, A., and Sherman, L. A. (1985) *Plant Physiol. 79*, 290−295.
5. Laudenbach, D. E., and Straus, N. (1988) *J. Bacteriol. 170*, 5018−5026.
6. Laudenbach, D. E., and Straus, N. A. (1992) *J. Gen. Microbiol. 138*, 1613−1621.
7. Hutber, G. N., Hutson, K. G., and Rogers, L. G. (1977) *FEMS Microbiol. Lett. 1*, 193−196.
8. Burnap, R. L., Troyan, T., and Sherman, L. A. (1993) *Plant Physiol. 103*, 893−902.
9. Falk, S., Samson, G., Bruce, D., Hunter, N. P. A., and Laudenbach, D. A. (1995) *Photosynth. Res. 45*, 51−60.
10. Bricker, T. M., and Frankel, L. K. (2002) *Photosynth. Res. 72*, 131−146.
11. Bibby, T. S., Nield, J., and Barber, J. (2001) *Nature 412*, 743−745.
12. Boekema, E. J., Hifney, A., Yakushevska, A. E., Piotrowski, M., Keegstra, W., Berry, S., Michel, K. P., Pistorius, E. K., and Kruip, J. (2001) *Nature 412*, 745−748.
13. Zouni, A., Witt, H. T., Kern, J., Fromme, P., Krauss, N., Saenger, W., and Orth, P. (2001) *Nature 409*, 739−743.
14. Vasilev, S., Orth, P., Zouni, A., Owens, T. G., and Bruce, D. (2001) *Proc. Natl. Acad. Sci. U.S.A. 98*, 8602−8607.
15. Bibby, T. S., Nield, J., and Barber, J. (2001) *J. Biol. Chem. 276*, 43246−43252.
16. Andrizhiyevskaya, E. G., Schwabe, T. M. E., Germano, M., D'Haene, S., Kruip, J., van Grondelle, R., and Dekker, J. P. (2002) *Biochim. Biophys. Acta 1556*, 265−272.
17. Guikema, J. A., and Sherman, L. A. (1983) *Plant Physiol. 73*, 250−256.
18. Sherman, D. M., and Sherman, L. A. (1983) *J. Bacteriol. 156*, 393−401.
19. Ruprecht, J., and Nield, J. (2001) *Prog. Biophys. Mol. Biol. 75*, 121−164.
20. Bricker, T. M., Morvant, J., Masri, N., Sutton, H., and Frankel, L. K. (1998) *Biochim. Biophys. Acta 1409*, 50−57.
21. Hankamer, B., Morris, E. P., Nield, J., Carne, A., and Barber, J. (2001) *FEBS Lett. 504*, 142−151.
22. van Heel, M., Gowan, B., Matadeen, R., Orlova, E. V., Finn, R., Pape, T., Cohen, D., Stark, H., Schmidt, R., Schatz, M., and Patwardhan, A. (2000) *Q. Rev. Biophys. 33*, 307−369.
23. van Heel, M., Harauz, G., Orlova, E. V., Schmidt, R., and Schatz, M. J. (1996) *J. Struct. Biol. 116*, 17−24.
24. van Heel, M. (1987) *Ultramicroscopy 21*, 111−124.
25. Jones, T. A., Zou, J.-Y., Cowan, S. W., and Kjeldgaard, M. (1991) *Acta Crystallogr. 47*, 110−119.
26. Jordan, P., Fromme, P., Witt, H.-T., Klukas, O., Saenger, W., and Krauss, N. (2001) *Nature 411*, 909−916.
27. Hankamer, B., Morris, E. P., Orlova, E., and Barber, J. (2001) *J. Struct. Biol. 135*, 262−269.
28. Gobets, B., van Stokkum, I. H. M., Rögner, M., Kruip, J., Schlodder, E., Karapetyan, N. V., Dekker, J. P., and van Grondelle, R. (2001) *Biophys. J. 81*, 407−424.
29. Byrdin, M., Jordan, P., Krauss, N., Fromme, P., Stehlik, D., and Schlodder, E. (2002) *Biophys. J. 83*, 433−457.
30. Golbeck, J. H. A. (1994) in *Molecular Biology of Cyanobacteria* (Bryant, D. A., Ed.) pp 193−196, Kluwer Academic Press, Dordrecht, The Netherlands.
31. Sétif, P. (2001) *Biochim. Biophys. Acta 1507*, 161−179.
32. Mühlenhoff, U., Kruip, J., Bryant, D. A., Rögner, M., Sétif, P., and Boekema, E. (1996) *EMBO J. 15*, 488−497.
33. Chitnis, V. P., and Chitnis, P. R. (1993) *FEBS Lett. 336*, 330−334.
34. Melkozernov, A. N., Lin, S., Bibby, T. S., Barber, J., and Blankenship, R. E. (2003) *Biochemistry* (in press).
35. Kamiya, N., and Shen, J.-R. (2003) *Proc. Natl. Acad. Sci. U.S.A. 100*, 98−103.

BI026933K